Road Materials and Pavement Design

ISSN: (Print) (Online) Journal homepage: https://www.tandfonline.com/loi/trmp20

Fourier-transform infrared analysis and interpretation for bituminous binders

Laurent Porot, Virginie Mouillet, Alexandros Margaritis, Hamzeh Haghshenas, Michael Elwardany & Panos Apostolidis

To cite this article: Laurent Porot, Virginie Mouillet, Alexandros Margaritis, Hamzeh Haghshenas, Michael Elwardany & Panos Apostolidis (2022): Fourier-transform infrared analysis and interpretation for bituminous binders, Road Materials and Pavement Design, DOI: 10.1080/14680629.2021.2020681

To link to this article: https://doi.org/10.1080/14680629.2021.2020681

Published online: 03 Jan 2022.

ROAD MATERIALS AND PAVEMENT DESIGN
https://doi.org/10.1080/14680629.2021.2020681

Taylor & Francis
Taylor & Francis Group

Fourier-transform infrared analysis and interpretation for bituminous binders

Laurent Porot [a], Virginie Mouillet[b], Alexandros Margaritis[c], Hamzeh Haghshenas[d], Michael Elwardany[e] and Panos Apostolidis [f]

[a]Kraton Polymers B.V., Amsterdam, the Netherlands; [b]Research team DIMA, Cerema Méditerranée, Aix en Provence, France; [c]Belgian Road Research Centre BRRC, Sterrebeek, Belgium; [d]University of Nebraska–Lincoln, Lincoln, NE, USA; [e]Western Research Institute WRI, Laramie, WY, USA; [f]Delft University of Technology, Delft, the Netherlands

ABSTRACT

InfraRed spectrometry is a powerful technique to characterise bituminous binders. The methodology is not fully harmonised and may lead to variability. The RILEM-272-PIM-TG1, evaluated seven complex bituminous, for which eleven laboratories performed FTIR. While, the spectra showed similar trends, further analysis was needed to improve comparison. A specific approach was applied on two binders, unmodified and polymer modified bitumen, and two ageing conditioning. Combining a Gaussian distribution and derivative analysis confirmed a good alignments of laboratory results. A two-step model was developed improving further interpretation. It consists of a baseline adjustment with eight points and normalisation over the maximum aliphatic peak. Furthermore, a specific fingerprint model was determined with the main absorption peaks defined by their location and shape. Only the intensity varies from laboratory to laboratory and binders. This general approach can be used as a platform to characterise aging or binder complexity.

ARTICLE HISTORY
Received 13 June 2021
Accepted 15 December 2021

KEYWORDS
Bitumen; asphalt; polymer modified bitumen; FTIR

Introduction

The asphalt industry has used more and more physical and chemical modifiers over the last two decades to adjust or enhance material properties. Such modifiers may be liquid additives or polymer-based, viscous, or solid particles. As a result, binders, used for asphalt application, are becoming even more complex materials, exhibiting potential multi-phase morphologies. In this context, the RILEM TC 272 PIM task group 1, TG1, 'Phase and Interphase behaviour of innovative bituminous Materials', focused on the suitability of testing methods for complex bituminous binders (Porot, Chailleux, et al., 2020). RILEM is an international non-profit organisation for experts and laboratories on materials. It stands for Réunion International des Laboratoires et Experts en Matériaux, international collaboration between laboratories and experts in materials. It was founded in June 1947 with the aim to promote scientific cooperation in the area of construction materials and structures. Its activities are regrouped in clusters, with cluster F dealing with Bituminous Materials and Polymers. Each cluster has Technical Committees on a specific subject matter with a lifetime of 5 years and within each TC, Task Groups, TG, are working on specific activities. The TC 272 PIM started in 2016 and was expected to end in 2021, with 17 participating laboratories. The experimental plan included seven bituminous binders in two groups: the polymer modified and liquid additives groups. The testing programme was run between

CONTACT Laurent Porot Laurent.porot@kraton.com

April 2019 and April 2020 with various tests performed, including chemical, thermal, microstructural, and physical characterisation (Apostolidis et al., 2021; Porot et al., 2021). Amongst these tests, Fourier Transform Infra-Red, FTIR, spectroscopy was performed by eleven laboratories on the different binders at different ageing conditions.

FTIR is a reliable and well-recognised analytical technique widely used to identify functional groups of organic molecules and mineral products. Matter molecules are excited by an electromagnetic wave in the mid-infrared region, approximately 4000 to 400 cm^{-1}. When a molecule absorbs electromagnetic radiation, there is an increase in its total energy. According to the quantum theory, only a quantum of radiation of specific energy can be absorbed by a molecule, thereby raising its energy from the ground state to an excited state. Infrared radiation is of sufficient energy to cause transitional, rotational, and vibrational energy levels of a molecule. Each vibration mode corresponds to a wavelength or absorption energy. Therefore, according to the wavelength, the analysis of the light absorption corresponds to a specific spectrum of a molecule, an ion, or a crystallised structure and can be considered as a digital fingerprint of the molecule.

The position of the wavelength peak provides information about the structure of this molecule in the sample and its concentration. The peak width is sensitive to the chemical matrix of the sample and the strength of the intermolecular interactions, including pH and hydrogen bonds. The broader the peak, the stronger the bond is.

Absorbance and transmittance are mathematically related to each other as in Equation (1)

$$A = -\log_{10} T \tag{1}$$

where A is the absorbance and T the transmittance.

Conversion does not modify the peak wavelength number. In literature, spectra are usually plotted in both modes. According to Beer's law, absorbance is proportional to the concentration as in Equation (2)

$$A(x) = \log\left(\frac{I_0}{I}\right) = \varepsilon_i(x) \cdot l \cdot c_i \tag{2}$$

where $A(x)$ is the absorbance for a wavelength number x, I_0 and I are the intensities of the incident light and transmitted light, respectively, $\epsilon_i(x)$ is the molar attenuation coefficient or absorptivity of the attenuating species, l is the optical path length, and c_i is the concentration of the molecule inside the solution. Then, to identify unknown groups or to make a comparison between spectra, absorbance or transmittance modes may be used. As the absorbance is proportional to the concentration, it can be used easier for quantitative analyses.

FTIR spectroscopy is one technique that offers reliable information on the chemical structures for bituminous binders, such as aliphaticity, aromaticity, oxygenation rate (Glaser et al., 2015; Lamontagne et al., 2001). However, as for all kinds of materials, attention is required to bitumen sample preparation in order to obtain a good quality Infrared (IR) spectrum. Traditionally, FTIR spectroscopies have been used to analyse bitumen by means of transmitting the IR radiation directly through the sample, laid in a film-shaped on a thin plate, transparent to the infrared radiations (CsI, KBr, NaCl, Sodium Chloride (NaCl), Potassium Bromide (KBr), Cesium Iodide (CsI) amongst others). However, in recent years, the technique of Attenuated Total Reflectance (ATR) has revolutionised solid sample analyses mitigating the most challenging aspects of IR analyses, namely sample preparation, consisting of laying the sample on a reflectance crystal, without any special dissolution or spreading on wafer KBr (potassium bromide). This operation improves the sample preparation time significantly.

An ATR accessory operates by measuring the changes in an internally reflected IR beam when the IR light comes into contact with a sample. An IR beam is directed onto an optically dense crystal with a high refractive index at a certain angle. This internal reflectance creates an evanescent wave that extends beyond the surface of the crystal into the sample held in contact with the crystal. It can be easier to think of this evanescent wave as a bubble of IR that sits on the surface of the crystal. This evanescent wave protrudes only a few microns (0.5 μm – 5.0 μm) beyond the crystal surface and into

the sample. Consequently, there must be good contact between the sample and the crystal surface. The evanescent wave will be attenuated or altered in regions of the IR spectrum where the sample absorbs energy. The attenuated energy from each evanescent wave is passed back to the IR beam, exiting the opposite end of the crystal and passed to the detector. The system then generates a typical IR absorption spectrum.

That ATR is a widely used method in the industry. However, this technique allows only a superficial part of the sample to be examined. One of the essential ATR parameters is the homogeneity of the physical contact between the sample and the crystal. It is difficult to reproduce the same quality of contact from experiment to experiment, making it problematic to obtain consistent quantitative results. Moreover, when measuring solids by ATR, it is essential to ensure good optical contact between the sample and the crystal. The available accessories clamp the sample to the crystal surface and apply pressure. ATR works well with elastomers and other deformable materials and fine powders, but many solids give very weak spectra because the contact is confined to small areas. The effect of poor contact is more significant at shorter wavelength numbers where penetration depth is low. The issue of solid sample/crystal contact has been mainly overcome by introducing ATR accessories with very small crystals, typically about 2 mm across. The most frequently used small crystal ATR material is diamond because it has high durability and chemical inertness. These small area ATR crystal top-plates generally provide only a single reflection, but this is sufficient if only the spectrometer displays shallow noise levels. The refractive index of the crystal is significantly greater than that of the sample, or else internal reflectance will not occur – the light will be transmitted rather than internally reflected in the crystal. Typically, ATR crystals have refractive index values between 2.38 and 4.01 at 2000 cm^{-1}. Thus, it can be assumed that the majority of solids and liquids have much lower refractive indices.

One drawback of ATR is that the method presents a lower signal-to-noise ratio than the total transmission methods (Glaser et al., 2015). Only the surface to a few μm is concerned with reflection, and the depth may vary with the wavelength number. Modern measurement devices have algorithms to correct wavelength but not always the same refraction index at each wavelength number. Thus, it has been a subject of research to improve the repeatability and reproducibility of measurement, which is related to the features of the ATR method.

FTIR has been used for almost 50 years to characterise bituminous binders (Dorrence et al., 1974; Petersen, 1986) and ATR mode being identified as an easy and reliable way of the experiment (Jemison et al., 1992). For example, it enables to address the formation of oxygenated groups upon ageing (Petersen, 1975). Frameworks were developed to quantify changes in specific functional groups in bitumen (Lamontagne et al., 2001), such as carbonyl and sulfoxide groups, related to bitumen ageing (Lopes et al., 2016). It is also used to quantify modification, especially for polymer modified bituminous binders (Adams et al., 2019; Masson et al., 2001) and as well for other additives (Weigl et al., 2021). Standard test methods have been developed, such as ASTM E168 (ASTM, 2016) in North America or Testing Method T521 in Australia (Roads & Maritime Services, 2012) to determine and quantify modifiers in bitumen.

Proposed quantification methods are very popular among the asphalt and bitumen research community. Moreover, various quantification methods have been developed, such as the LCPC (Mouillet et al., 2009) or the BRRC (Pierard, 2013) methods. Most methods consider the same approach, using a tangential valley-to-valley quantification method, with a difference in normalisation steps and wavelength limits.

The Task Group 5, TG5, of the TC-206 ATB (Partl et al., 2013), and later the TC-237 SIB (Partl et al., 2018) worked extensively on evaluating various methods, including those mentioned above. The aim was to provide an overview of the existing quantification approaches and their differences in terms of results, in an attempt to provide universal ageing indicators for aged bituminous binders. Their work pointed out that different methods show significantly different results, and harmonising the acquisition procedure will significantly improve the characterisation efficiency of bituminous binders.

Later, the TC-252 CMB worked on a round-robin test investigating the effect of short-term ageing conditioning temperature of bitumen and included reproducibility of FTIR measurements (Hofko et al.,

2014). Within this experimental programme, four different sources of the same penetration grade bitumen were evaluated, considering both short- and long-term ageing binder laboratory conditioning. Two integration methods, baseline and tangential, and two correction methods, no correction and correction with baseline adjustment, were considered.

Research objectives

Investigating the chemical composition of bitumen using FTIR spectra requires an accurate post-processing procedure of the acquired spectra. The motivation of this study was first to present the variability among the spectra of the inter-laboratory campaign and second, to propose a simple modelling approach for the harmonisation of the spectra. For this purpose, the combination of the Gaussian distribution and derivative analysis of the main absorption peaks and their limits was used to assess the reproducibility of measurements between all laboratories. A simple fitting model was introduced to improve the comparison between laboratory results. Finally, a typical fingerprint for bitumen was determined. These approaches will enable later to better process IR spectra, either related to ageing or explicitly associated with the presence of modifiers.

Experiment plan

Materials

The RILEM PIM TG1 evaluated seven binders, one group with polymer modification and another group for liquid additives, including neat bitumen as used for reference comparison. Table 1 provides the list of all materials with respective grading.

The two neat bitumen were from the same source, with Bit1 having similar consistency to the PMBs at intermediate temperature, based on penetration value at 25°C, and the Bit2 being used to produce the PmB2.

The choice of the PmB was made to have two significantly different binders. The PmB1 was a commercially produced PmB, and also used in the RILEM PIM TG2, looking at asphalt mix characteristics. The PmB2 was a laboratory-produced PmB with 7.5% of high vinyl linear SBS polymer, ensuring a rich polymer phase to enhance rutting and fatigue properties; its base bitumen was Bit2.

The choice of the liquid additives was made to have different additives by nature. Blend1 was made with bio-based additive classified as asphalt reuse/recycling additive and being already evaluated in RILEM TC 264 RAP (Cannone Falchetto et al., 2019; Porot, Huguener, et al., 2020), with a dosage of 4%. Blend2 was made with a petroleum-based additive, described as Refined Engine Oil Bottom, used as a softener with a dosage of 8%. Blend3 was with liquid paraffinic oil, most likely not used in paving applications, with a dosage of 4% per weight. The three blends were made to target similar consistency to the Bit2.

Table 1. List of materials evaluated in RILEM PIM TG1.

Label	Binder	Pen grading	PG grading
Bit1	Neat bitumen 35/50	35/50	PG 70-22
PmB1	Standard PmB	25-55/70	PG 76-16
PmB2	Highly modified PmB	25-55/85∗	PG 82∗-28
Bit2	Neat bitumen 70/100	70/100	PG 64-22
Blend1	Bit1 + bio-based additive	70/100	PG 64-28
Blend2	Bit1 + REOB	70/100	PG 64-28
Blend3	Bit1 + paraffinic oil	70/100	PG 64-28

∗Measured values were higher than the maximal class from respective specification.

Table 2. Experimental matrix with laboratory participation for FTIR measurement.

	Bit1	PmB1	PmB2	Bit2	Blend1	Blend2	Blend3	Original	RTFOT	PAV
Total	8	8	9	9	7	7	7	11	7	8
Lab1	x	x	x	x	x	x	x	x	x	x
Lab2	x	x	x	x		x		x		
Lab5	x	x	x	x				x	x	x
Lab6	x	x	x	x	x	x	x	x	x	x
Lab7				x	x	x	x	x	x	x
Lab8	x	x	x					x	x	x
Lab10			x	x				x	x	x
Lab12	x	x	x	x	x	x	x	x		x
Lab14	x	x	x	x	x	x	x	x		
Lab15					x	x	x	x	x	x
Lab16	x	x	x	x	x		x	x		

Table 3. FTIR protocol for each laboratory.

Lab	Mode	Equipment	Crystal	Software	Scan	Resolution	Replicates
1	ATR	PerkinElmer	Diamond	PerkinElmer	64	4	1
2	ATR	PerkinElmer	Diamond	PerkinElmer	8	2	2
5	ATR	PerkinElmer	Diamond	N.R	24	4	3
6	ATR	Bruker	Diamond	OPUS	24	4	2
7	ATR	Bruker	Diamond	OPUS	32	2	1
8	Transmittance	PerkinElmer	Diamond	Spectrum	32	4	3
10	ATR	Shimadzu		Shimadzu	45	4	1
12	Transmittance	PerkinElmer		Spectrum	4	4	1
14	ATR	Nicolet	Diamond	Omnic	32	4	3
15	ATR	Nicolet	Diamond	Omnic	4	4	2
16	ATR	Nicolet	Diamond	Omnic	32	4	1

Testing

The different binders were all artificially aged by each laboratory with short-term ageing, through Rolling Thin Film Oven Test, RTFOT, at 163°C according to EN 12607-1, and further with Pressure Ageing Vessel, PAV, for 20 h at 100°C, according to EN 14769. At the different ageing conditioning, the binders were extensively tested by the different laboratories with conventional properties and more fundamental properties measurements (Porot et al., 2021). More specifically, for FTIR, eleven laboratories did measurements, but not necessary on all binders and all ageing conditioning. Table 2 shows the experimental matrix for each binder, with the total number of results collected for FTIR measurements. The laboratories, which are not numbered in the table, participated in the RILEM PIM TG1 but did not perform FTIR. In total, each binder was evaluated by seven to nine different laboratories, for which eleven laboratories performed measurement on the original binder, seven after RTFOT and eight after RTFOT + PAV.

Table 3 provides an overview of the different protocols used by each laboratory. Most of them did FTIR in Attenuated Total Reflectance, ATR, between 4000 and 600 cm^{-1} with 32 scans and a resolution of 4 cm^{-1} using diamond crystal.

Overall results

A total of 122 spectra were collected from all laboratories. Figure 1 provides an example of the seven binders in the original stage. For each binder at each ageing conditioning, the spectra were compared between all laboratories. Only one laboratory computed the raw data prior to sharing them, using an internal protocol to adjust the baseline and normalise the spectrum; it is shown in blue with the highest spectrum.

Overall, spectrum variability was observed between laboratories, but all spectra displayed similar absorption peaks. Scatter can be observed on the baseline, although two groups can be noticed, and some variations can be noticed for the maximum value of the peaks. As a quick comparison between binders, some differences in absorption peaks can already be identified. For example, with PmB's, some additional absorption peaks, compared to neat bitumen, are visible around

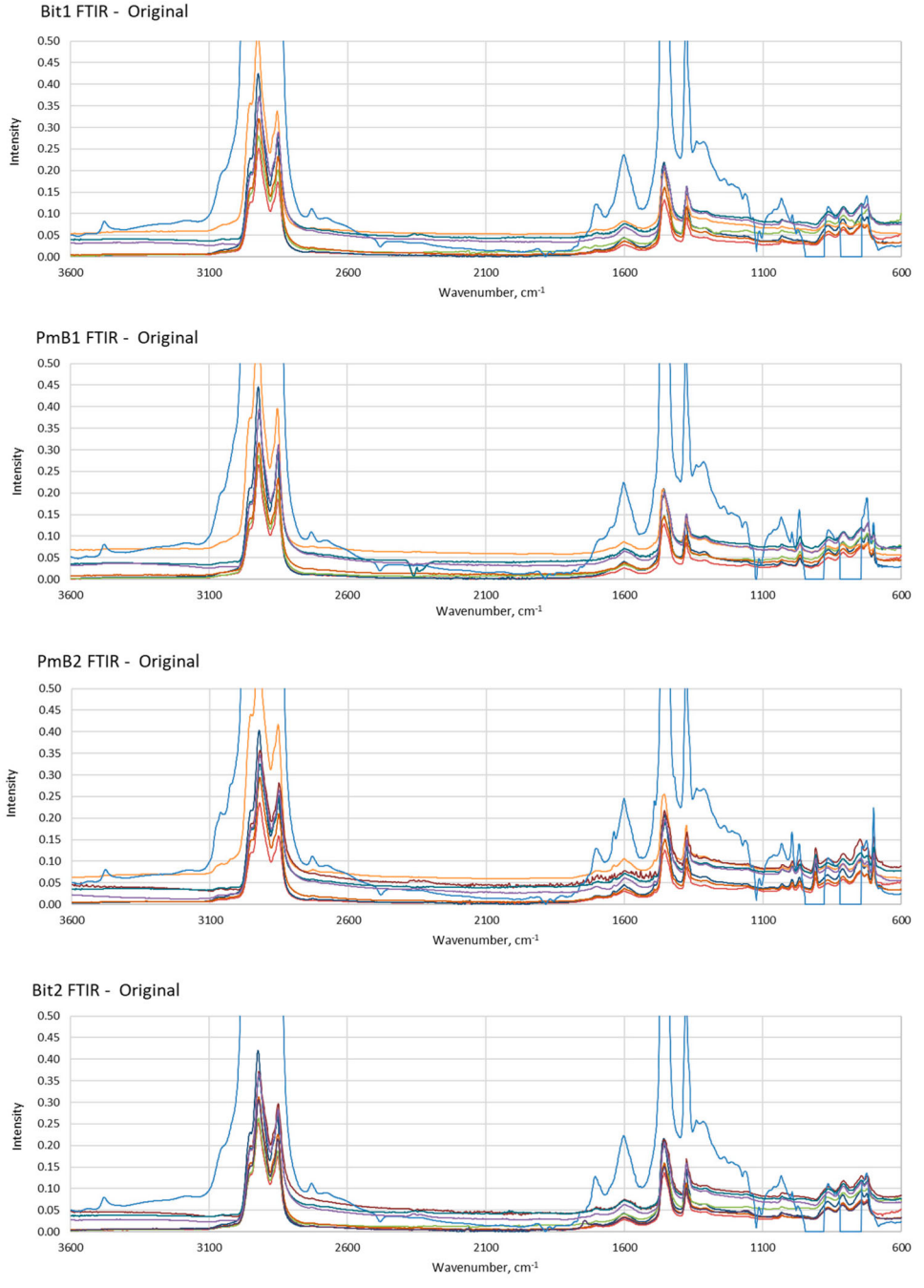

Figure 1. FTIR spectra for the seven original binders.

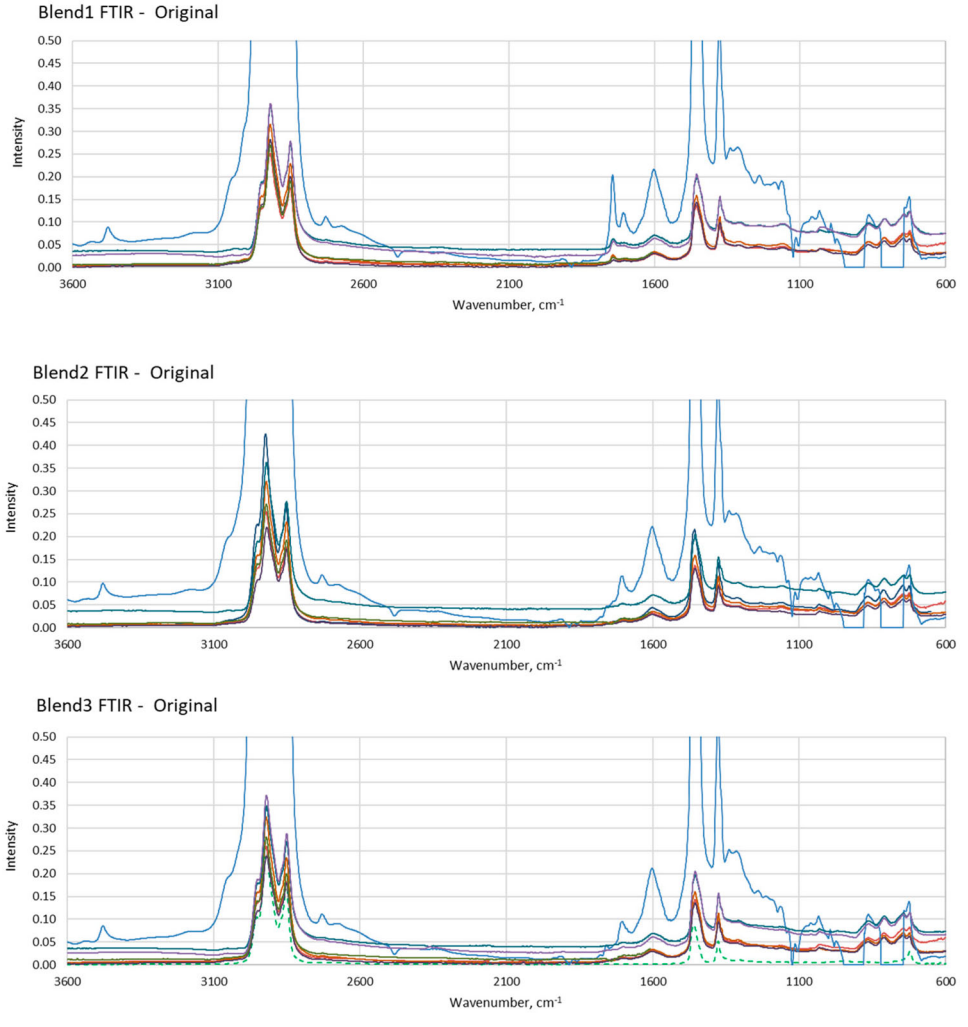

Figure 1. Continued.

700, 910, 960 cm^{-1}. And for Blend1 additional absorption peak around 1740 cm^{-1} was observed as well. For simplicity, Bit1 and PmB2 were selected for further analysis and discussion later in this paper.

Analysis of the data

The first quick analysis of the measurements is visual, where peaks can clearly be identified and located. With location, the height and width can characterise the absorption peaks. Beer's law, Equation (2), assumes the concentration is proportional to the total absorbance related to the intensity of the absorption peak. Thus, a model to determine and quantify the height will help in interpreting spectra. Most FTIR equipment and software include deconvolution options to model spectrum. This is often based on normal Gaussian distribution or Lorentzian or a combination of both. Although it has been shown that the Lorentzian band shape is more accurate than Gaussian and mixed Lorentzian–Gaussian band shapes (Abramowitz & Bauman, 1963; Seshadri & Norman,

1963). The difficulty is in determining the degree of deconvolution. With complex materials having multiple species, an infinite of peak combination and overlapping is often observed. Modelling all of them is an endless process and does not necessarily improve the accuracy of the interpretation. Thus, deconvolution would need to be wisely done and tailored to the materials and mains species.

Normal distribution

The theory for normal Gaussian distribution postulates that the probability for species to answer to wavelength number is equal before or after the absorption peak, as in a bell shape. Gaussian distribution follows the law as in Equation (3).

$$f(x) = \frac{1}{\sigma\sqrt{2\pi}} e^{-1/2\left(\frac{x-x_0}{\sigma}\right)^2} \tag{3}$$

and hence, its 1st derivative is defined as

$$f'(x) = -\frac{1}{\sigma\sqrt{2\pi}} \frac{x-x_0}{\sigma^2} e^{-1/2\left(\frac{x-x_0}{\sigma}\right)^2} = -\frac{(x-x_0)}{\sigma^2} f(x) \tag{4}$$

where x_0 is the central value and σ standard deviation representative of the shape of the bell curve.

From that, it is worth noticing that:

- At $x = x_0$, $f(x_0)$ is maximum, $f(x_0) = \frac{1}{\sigma\sqrt{2}}$
- At $|x-x_0| = \sigma$ the derivative is max / min, this is the inflexion point of the curve, and $f(x_0 + / - \sigma) \cong 0.6/\sigma\sqrt{2\pi} \cong 0.6 f(x_0)$
- At any given value of σ, the total area is equal to 1, $\Sigma f(x) = 1$, the total area is independent of the width / shape of the curve.

This implies that the difference in absolute value between the peak and the inflexion values is 40% of the maximum value. In other words, when applied to IR spectra, knowing the difference between the maximum and inflexion absorbance values enables to calculate the total area of the specific absorbance as

$$\text{Area} = \sqrt{2\pi} \cdot \left(\frac{y_{\max} - y_{\text{infl}}}{0.4}\right) \cdot (x_{\max} - x_{\text{infl}}) \tag{5}$$

where y is the absorbance values, x is the wavelength number, and max / infl are the maximum and inflexion points. In addition, the location of the inflexion point is independent of the total area of the curves. Then for a given σ the total area is proportional to the intensity of the absorption peak. Figure 2 shows an example of two Gaussian curves having the same standard deviation but different total areas and their respective derivatives below. Inflexion points are located at the same location regardless of the total area.

Another way is to consider the area of the 1st derivative. Between two points, the area is equal to the integral of the 1st derivative between these two points, in other words, the difference of values between the two points defines the area of the 1st derivative.

$$\text{Area} = \int_{x1}^{x2} f'(x)dx = f(x2) - f(x1) \tag{6}$$

This can apply either from the inflexion point to the max of the peak or between the points where the 1st derivative is null, as illustrated in Figure 3.

The 2nd derivative is also sometimes considered and will help to locate the peaks of the 1st derivative. In other words, the number and position of IR bands can be determined by the minimum of the 2nd derivative of spectra (Maddams, 1980).

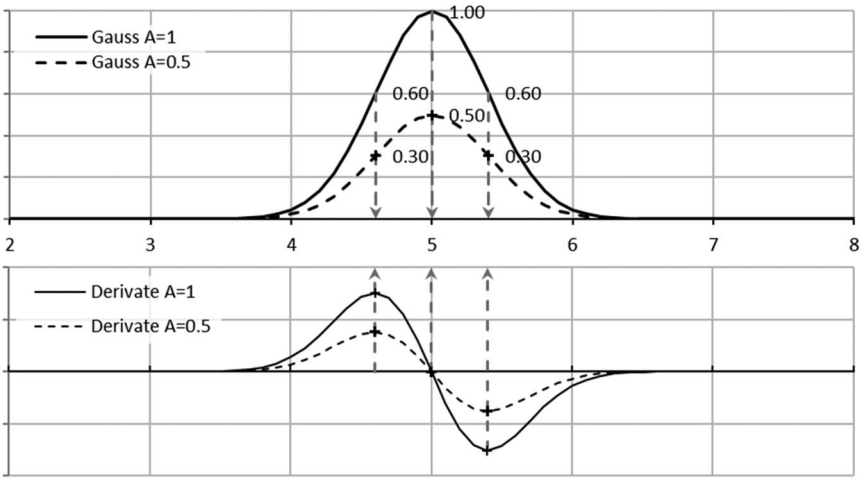

Figure 2. Example of normal Gaussian distribution and its derivative.

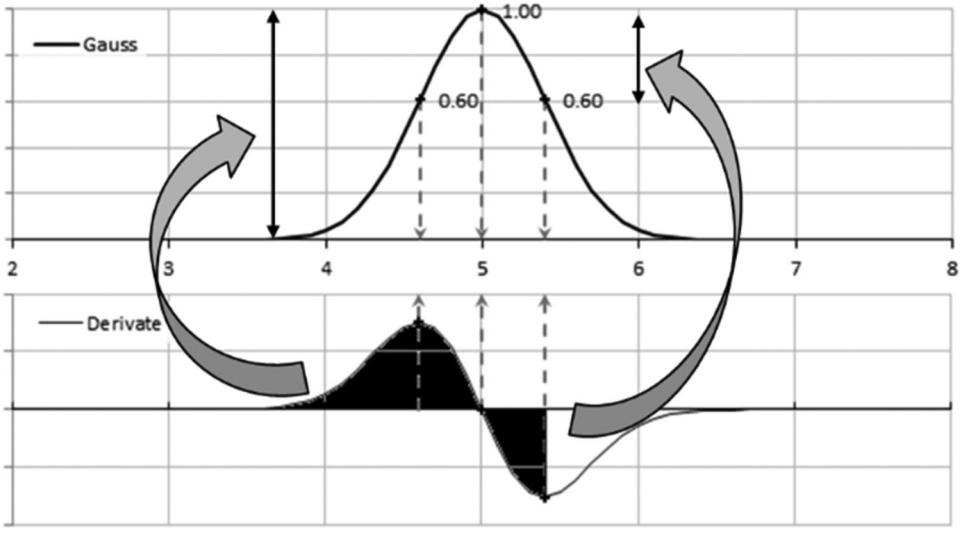

Figure 3. Relation between derivative area and height of a peak.

Peak analysis

Deconvolution based on Gaussian normal distribution, applied to IR spectra, can help identify the different absorption peaks and in an absolute way to model the spectra. Peaks are located when the 1st derivatives are equal to zero and then the max or min of the derivative corresponds to the inflexion points. One advantage of the use of the 1st derivative of the spectra is to eliminate any difference in baselines. Figure 4 displays the 1st derivatives of the spectra for Bit1 and PmB2 with seven and eight different laboratories, respectively. Lab2 showed a wide variation due to the resolution of the signal, which was 2 cm^{-1} as compared to 4 cm^{-1} for the remaining. Lab16 reported wavelength every 0.5 cm^{-1} as compared to others reporting every 1 cm^{-1}, which generated more noise in calculating the derivatives. While some differences in intensity of the 1st derivatives of the spectra for all laboratories can be observed, the points where derivatives crossed the zero line and the min / max values, are positioned at the same wavenumbers. For all laboratories, the signals are consistent and the spectrum

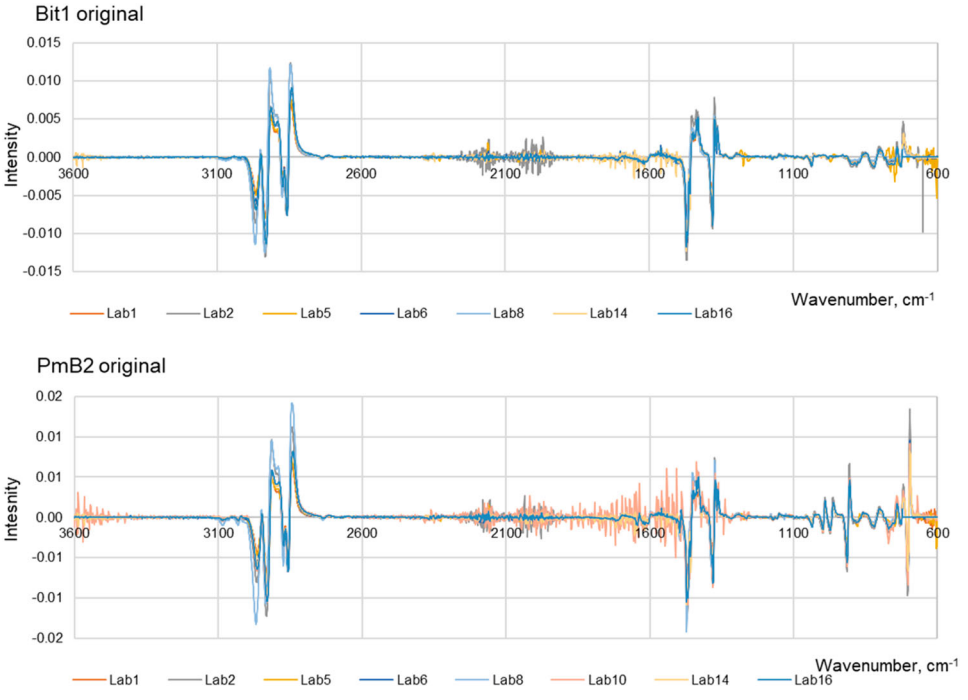

Figure 4. 1st derivatives of IR spectra of Bit1 and PmB2 from different laboratories.

Table 4. Location of absorption peaks based on derivative analysis, cm^{-1}.

Bit1				PmB2			
average	st dev	min	max	average	st dev	min	max
2922	2.63	2920.5	2927	2921	1.70	2920.5	2924
2853	2.42	2851	2858	2853	2.64	2851	2859
1601	1.56	1599	1603	1601	0.93	1600	1602
1457	1.81	1455	1460	1456	0.98	1454	1457
1376	0.68	1375	1377	1376	0.81	1375	1377
1032	0.79	1031	1033	1031	0.75	1030	1032
				994	0.55	993	995
				967	0.89	966	969
				910	3.31	909	919
864	1.66	863	867	866	2.59	864	872
811	3.52	809	819	811	3.23	808	819
				699	0.50	698	699

shapes are similar, only displaying differences in baselines and relative intensities. This is valid for both neat bitumen, Bit1, and complex PmB, PmB2.

The interpretation of the derivatives helps to determine the location of the most relevant absorption peaks. Table 4 shows the average values as specified for both Bit1 and PmB2. This analysis helps to define specific fingerprints for the most common neat bitumen. In general, variations between laboratories are less than 2 cm^{-1}. When the standard deviation is greater than 1.5, as highlighted in grey in the table, it came from one single laboratory reporting value out of range of the other ones. Worth noticing that for the lower wavenumbers, between 600 and 900 cm^{-1}, more variations are observed, and peaks are difficult to isolate.

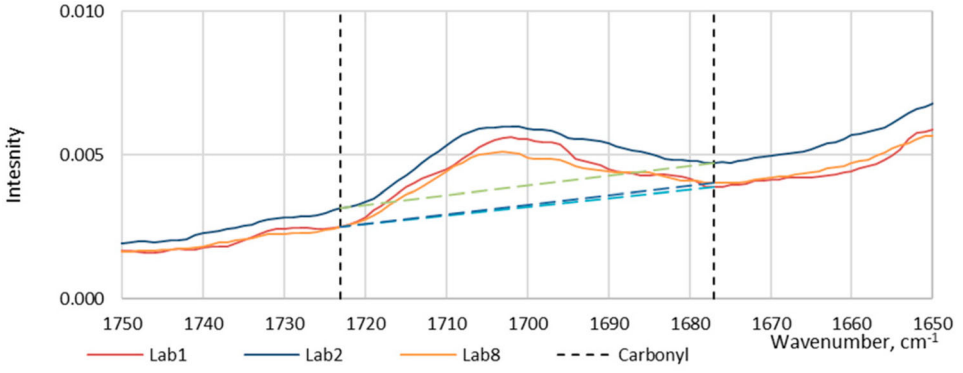

Figure 5. Example of determination of boundaries around 1700 cm^{-1} for Bit1.

Table 5. Boundaries for Bit1 original by manual interpolation, cm^{-1}

Band	C = O		S = O		CH2, CH3	
Limit	lower	upper	lower	upper	lower	upper
Lab1	1723	1677	1049	985	1520	1330
Lab2	1723	1677	1049	985	1520	1330
Lab5	1723	1677	1049	985	1520	1330
Lab6	1718	1684	1049	987	1520	1330
Lab8	1723	1677	1048	987	1520	1330
Lab12	1728	1674	1049	982	1520	1330
Lab14	1719	1677	1047	985	1510	1330
Lab16	1720	1677	1049	985	1515	1330
Average Width	45		64		188	
Average	1722	1678	1049	985	1518	1330
St Dev	3.14	2.83	0.74	1.55	3.72	0.00
Min	1718	1674	1047	982	1510	1330
Max	1728	1684	1049	987	1520	1330

Boundary analysis

One way to interpret FTIR data is by determining indexes for specific functional groups using areas. The areas are determined around the absorption peak between defined boundaries where the spectra are flat. Figure 5 provides an example for the band around 1700 cm^{-1} for Lab1 and Lab5. Usually, these boundaries may vary from one binder to another, from one conditioning to another, or from one laboratory to another. They can be defined by visual observation by making use of the 'valley-to-valley' method, avoiding the integration of negative areas. The solution of fixed boundaries can homogenise the area calculation with a minimum time spent, especially when many spectra must be interpreted. However, it can lead to biased results due to the negative area in the calculation (Dony et al., 2016).

The analysis was done on Bit1 for all laboratories, with manual calibration of the boundaries for the C = O, S = O, and CH2 / CH3 groups. Table 5 gives the different boundaries for all laboratories. Overall, the variation between laboratories is relatively small, less than 5 cm^{-1} (except for Lab6 for C = O). The difference between the lower and upper limits was consistent among all laboratories, with 45 for C = O, 65 for S = O, and 188 cm^{-1} for CH2/CH3. However, it is worth mentioning that the exercise was done on the original binder for which the C = O and S = O are usually of weak intensity. The minor variations of limits of C = O could be due to some noisy spectra from insufficient atmospheric correction. This correction, which is not a mathematical treatment, must be used when focusing on a carbonyl-style OH peak at 1700 cm^{-1} to remove the contribution of CO_2 and H_2O vapour from the spectra bands.

Fitting model

Within the inter-laboratory experiments with FTIR, it was always a discussion comparing the spectra from different laboratories. RILEM already has a long record of such experiments, primarily when considering ageing and tracking oxidation phenomena. The RILEM TC 206-ATB TG5 in 2004–2010 (Partl et al., 2013) investigated binder recovered from laboratory-aged asphalt mixtures. FTIR data from eight laboratories was collected on binder aged at different levels from laboratory and plant produced mixes. The analysis was based on index calculation using the LCPC method (Mouillet et al., 2009) and repeatability was between 10% and 22%. The same data was further computed within the RILEM TC 237-SIB TG5 in 2010–2017 (Partl et al., 2018) by applying different methods to calculate and standardise the IR spectra to determine indexes. In this attempt, automatic deconvolution was used with promising outcomes to improve reproducibility (Marsac et al., 2014). However, the complexity of the method has not been further used in the next RILEM TCs.

The RILEM TC 252 CMB TG2 in 2013–2018 (Hofko et al., 2014) investigated the effect of short-term laboratory ageing on bituminous binders. The experiment was conducted with three different RTFOT temperatures and further PAV on four different sources of the same bitumen grade 70/100. Nine laboratories participated in the experiment, including FTIR data. Different methods to determine indexes were reviewed from valley-to-valley or from baseline adjustment. The need to calibrate the spectrum has been identified as a key point in comparing spectra from different laboratories. The recommendation was to adjust the baseline at the wavelength number of 1800 cm^{-1} and further use the area above the baseline. While it provided better reproducibility for the carbonyl index (Hofko et al., 2017), it presents the drawback of bias and minimises the area close to the baseline adjustment.

Other methods do exist. For example, the LCPC testing method 69 (Mouillet et al., 2009) has been established and successfully used for more than 10 years. It determines indexes based on the ratio of areas for carbonyl and sulfoxide groups over the aliphatic groups. The areas are defined on a valley-to-valley basis and it provides reasonably good repeatability and reproducibility. This method does not need refitting the spectra as any deviation of the baseline is offset when considering the valley-to-valley principle. The normalisation of the carbonyl/sulfoxide areas over the aliphatic ones also compensates for any scaling effect between spectra. This method has been successfully used within the MURE project in France from 2012 to 2018. The project looked at a full-scale evaluation of road trial sections combining warm mix and recycling techniques. Nine laboratories performed FTIR on a neat bitumen and three different binders as recovered from asphalt mixes containing Reclaimed Asphalt. The analysis used the LCPC method 69. The outcomes came with useful recommendations for sample preparation to perform FTIR measurements (Dony et al., 2016).

In Belgium, the Belgian Road Research Centre, BRRC, has also developed a specific method to standardise the spectrum and determine indexes (Pierard, 2013). The baseline is adjusted between 2000 and 400 cm^{-1} and the whole spectrum is then normalised to a maximum absorption peak intensity of 1.2, usually at 1458 cm^{-1}.

Further efforts were made to increase repeatability (Hofko et al., 2017) based on a neat and a polymer modified binder and eight different quantification procedures. The procedures varied based on three factors: original or normalised spectra, integration or absorbance maximum point and baseline or tangential integration. The findings showed that, for the neat binder, the best method in terms of repeatability was achieved when the baseline integration was used together with original and normalised spectra. It must be noted that integrating larger areas, as happens when considering the baseline approach, will naturally minimise the peaks close to the baseline adjustment point and thus artificially increase repeatability. The method was further optimised with additional baseline correction (Margaritis et al., 2020), bringing the absorbance at 1753 cm^{-1} at 0 and absorbance correction at 2923 cm^{-1} brought to 1, having the same absorbance intensity.

For simplicity, the fitting and analysis approach is discussed in detail for Bit1, but the same method was applied to both Bit1 and PmB2, and similar outcomes were observed.

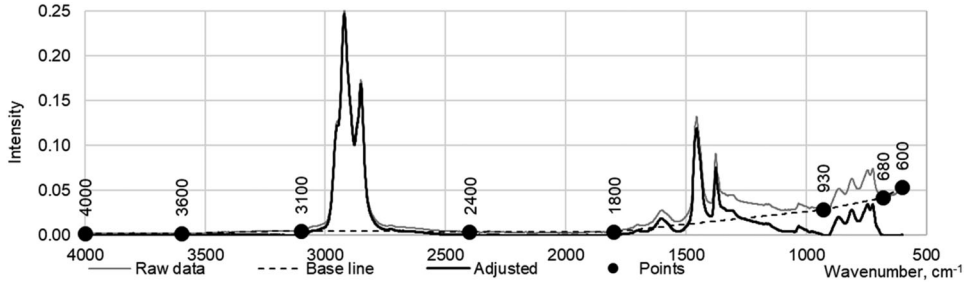

Figure 6. Baseline adjustment principle.

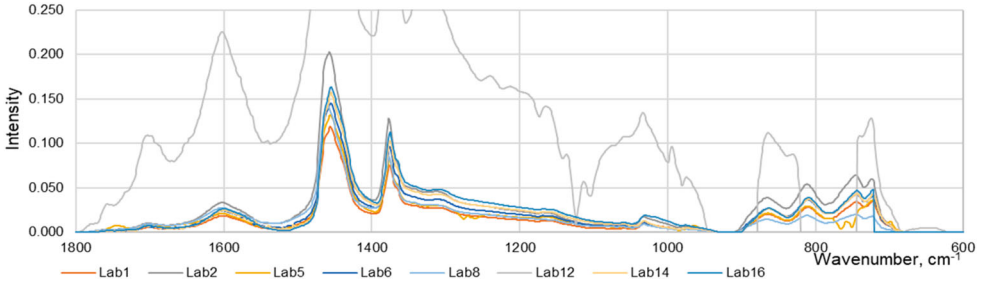

Figure 7. Baseline adjustment for Bit1 from measurements of 8 laboratories.

Baseline adjustment

The first adjustment was applied to shift the baseline. Along with the scanning, there is ineluctable interference between each peak, which leads to noise in the response, creating an accumulative variation of the baseline. Figure 1 showed the raw data for the results from the different laboratories. One laboratory already did adjustment and normalisation based on its internal procedure and, as a result, delivered a spectrum that had higher peaks. With the example of Bit1, two groups can be identified with lower vs. higher baseline starting already around 0.05 absorption intensity.

The baseline adjustment aimed to shift down the curve where intensities are almost constant or show a valley at zero as per Equation (7)

$$A_{\text{shifted}} = A_{\text{measured}} - a_i^{i+1} \tag{7}$$

where A_{shifted} is the shifted absorbance, A_{measured} is the measured absorbance, and a_i^{i+1} is the shifting correcting factor applied between wavelength number i and $i+1$.

For that, eight points were visually selected, as shown in Figure 6 with a dotted line. The line joining the different points was then subtracted from the raw spectra and with new 'adjusted' baseline spectra.

The same principle was applied to the results from all laboratories. Figure 7 displays the outcomes for the eight labs for spectra between 1800 and 600 cm^{-1}, as a most relevant zone for bitumen. As compared with Figure 1, there is a recordable improvement in the scatter between laboratories. However, variations in amplitude were still observed, especially for the laboratory that pre-adjusted and normalised the data.

Normalisation

The second step consists of the normalisation of the different baseline adjusted spectra, stretching the spectra as per Equation (8).

$$A_{\text{normalised}} = \beta \cdot A_{\text{shifted}} \tag{8}$$

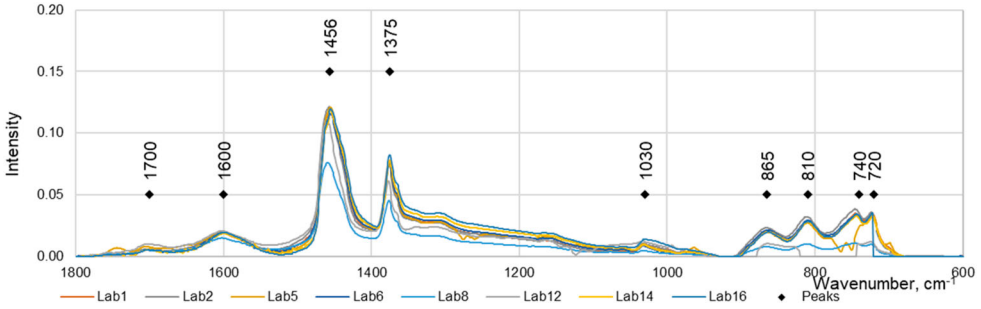

Figure 8. Normalisation A by maximum peak from 4000 to 600 cm^{-1} to 0.25 for Bit1, 8 laboratories.

where $A_{normalised}$ is the normalised absorbance and β is the stretching factor.

The intensity of the signal may be affected, amongst others, by the quality of the laser source; over time, it may lose some power reducing the signal intensity. For normalisation, four different approaches may be considered either by the sum of the areas over the whole spectrum or by the maximum intensity of absorption peaks. In reading the spectra, as shown in Figure 1, the peaks around 2950 and 2920 cm^{-1} are far the highest, and thus, normalisation based on them may minimise the other peaks and result in loss of sensitivity. Thus, four options for normalisation were considered:

- Normalisation A, by maximum peak from 4000 to 600 cm^{-1} to 0.25
- Normalisation B, by maximum peak from 1800 to 600 cm^{-1} to 0.15
- Normalisation C, by total area from 4000 to 600 cm^{-1} to 50
- Normalisation D, by total area from 1800 to 600 cm^{-1} to 25

Figure 8 shows the spectra after normalisation A, based on the maximum absorbance peak of the whole spectra between 4000 and 600 cm^{-1}. The maximum peak was located around 2920 cm^{-1} for all laboratories, with intensity varying between 0.25 and 2.73 and an average at 0.64. Thus, all baseline adjusted spectra were normalised to 0.25 intensity at 2920 cm^{-1}. For spectra between 1800 and 600 cm^{-1}, which is of more specific interest for bitumen analysis, there is less scatter between laboratories than in Figure 7. Especially the one, Lab14, which was pre-normalised, was now in the same order of magnitude as the others. However, some variations were still recordable between 1457 and 1100 cm^{-1}.

Figure 9 shows the spectra after normalisation B, based on the maximum absorbance of the spectra between 1800 and 600 cm^{-1}. The maximum absorption peak was located around 1456 cm^{-1} for all laboratories, with absorption intensity varying between 0.12 and 1.19 and an average at 0.28. Thus, all baseline adjusted spectra were normalised to 0.15 intensity at 1456 cm^{-1}. There was less scatter between laboratories at spectra between 1800 and 600 cm^{-1}, as compared to Figure 7 and even better than Figure 8. Only two laboratories were slightly out of range in the low wavelength zone.

Figure 10 shows the spectra after normalisation C, based on the total area of the whole spectra between 4000 and 600 cm^{-1}. The value varied between 41 and 467, and an average of 118. All baseline adjusted spectra were normalised to 50 for the total area. There was less scatter between laboratories at spectra between 1800 and 600 cm^{-1} than in Figure 7, but still higher than Figure 8, with one laboratory being below the other.

Figure 11 shows the spectra after normalisation D, based on the total area of the whole spectra between 1800 and 600 cm^{-1}. The value varied between 18 and 162 and an average of 45. All baseline adjusted spectra were normalised to 25 for the total area. The spectra between 1800 and 600 cm^{-1}, similarly to the normalisation C, showed less scatter between laboratories than in Figure 7, but still with more than one laboratory being below the other.

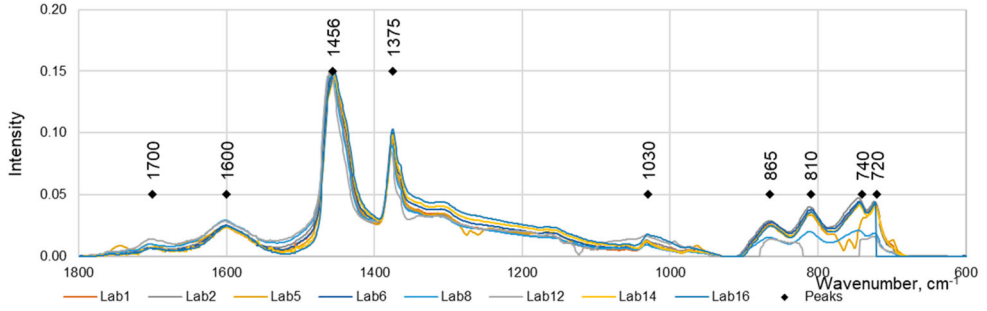

Figure 9. Normalisation B by maximum peak from 1800 to 600 cm^{-1} to 0.15 for Bit1, 8 laboratories.

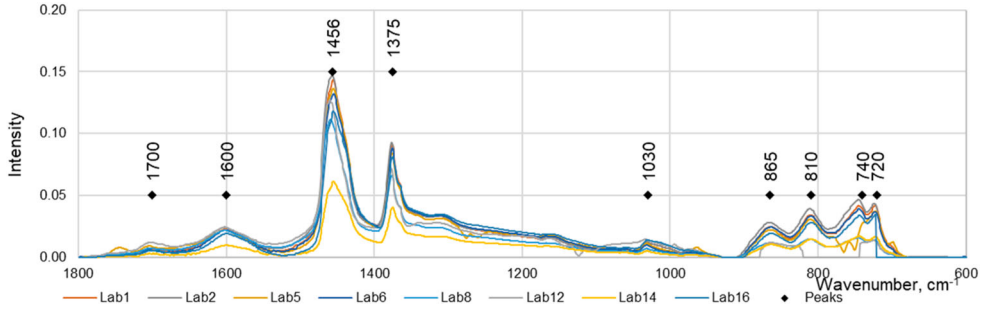

Figure 10. Normalisation C by total area from 4000 to 600 cm^{-1} for Bit1, 8 laboratories.

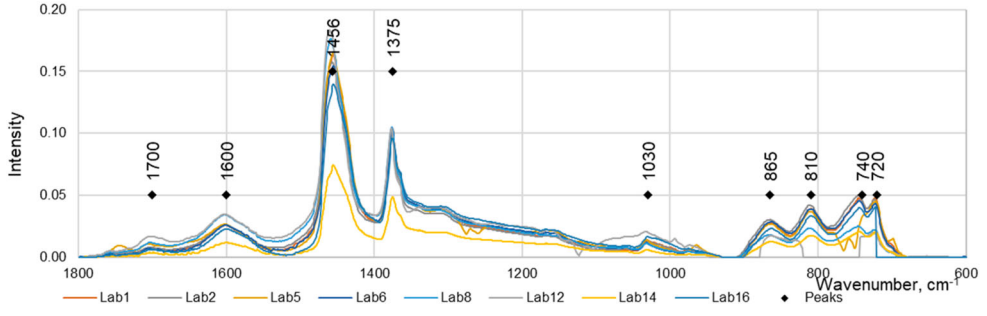

Figure 11. Normalisation D by total area from 1800 to 600 cm^{-1} to 0.25 for Bit1, 8 laboratories.

While the normalisation, based on the area, would have made more sense as the absorption peaks should be proportional to the concentration of the associated species, it does not improve the scatter compared to the normalisation based on absorption peak height. Then, depending on which part of the spectra is of interest for analysis, either one option or the other would be selected. When analysing bitumen and functional groups in bitumen, the trend is more apparent between 1800 and 600 cm^{-1}, especially when considering ageing or modification with SBS or bio-based products. Normalisation B is suggested as the preferred option.

Standardised FTIR data processing

Finally, the standardised procedure for FTIR analysis is proposed as follow:

(1) Baseline adjustment through the valleys at wavelength numbers 4000, 3600, 3100, 2400, 1800, 930, 680 and 600 cm^{-1}

$$A_{shifted} = A_{measured} - \left[A_i + \left(\frac{A_{i+1} - A_i}{w_{i+1} - w_i} \times (w - w_i)\right)\right] \quad (9)$$

where A_i and w_i being respectively the absorption intensity and the wavelength number, i and $i+1$ being the two consecutive adjustment points.

(2) Normalisation with the maximum peak intensity between 1800 and 600 cm^{-1} over 0.15

$$A_{normalised} = A_{shifted} \cdot \left(\frac{A_{max}|_{600}^{1800}}{0.15}\right) \quad (10)$$

The spectra of both binders, Bit1 and PmB2, were computed in the same way and presented in Figure 12 between 1800 and 600 cm^{-1}. The spectra for Bit1 after RTFOT + PAV ware also calculated mainly to determine impacts to the C = O and S = O functional groups.

FTIR fingerprinting approach

The use of the derivative enables identifying the main absorption peaks where the derivative is null, the absorption peak is at its maximal value. Moreover, the inflexion points, where the derivative is either maximal or minimal, can define the shape/width of the peaks. The fitting model for the various spectra confirmed reasonably consistent measurements between various laboratories in identifying the same absorption peaks and the same shape, at least for the two binders Bit1 and PmB2 investigated in detail.

Bituminous binders contain many different components and are difficult to qualify with a limited number of molecules. Thus, with FTIR, the interpretation is even more complex and can lead to wide numbers of species leading to multiple absorption peaks. Automatic deconvolution, through device software, may lead to an infinite combination of solutions.

For bitumen, depending on the species foreseen, different wavelength numbers can be tracked (Pipintakos et al., 2020). Amongst others, the carbonyl and sulfoxide groups are of particular interest as related to variation over ageing. However, the carbonyls are of a broad family of multiple bonds in the range of 1740–1630 cm^{-1} (Geng et al., 2009). It includes, amongst other esters, acid groups such as carboxylic or naphthenic acids, ketones. Reducing the carbonyl group to solely oxidation may lead to misinterpretation. In the example of Bit1, by nature, it contains already naphthenic acid groups, which can be identified within the carbonyl bands. The sulfoxides are also a broadband of peaks and not always easy to isolate the one typically related to oxidation. With Polymer modification, it will be possible to identify specific absorption peaks (Mouillet et al., 2008). Within the scope of the study, the PmB were most likely modified with Styrene Butadiene Styrene. Specific peaks were identified at 990, 965, 910 and 700 cm^{-1} wavelength numbers. Similarly, when considering bio-based liquid additives, specific peaks can be identified (Oreskovic et al., 2020). With Blend1, a specific peak was identified around 1740 cm^{-1} as the ester group.

Then, combining the analysis of spectra, through derivative, Gaussian approach and the fitting model, with baseline adjustment and normalisation, it was possible to identify the main absorption peaks and propose a typical fingerprint for bituminous binders. To isolate single absorption peaks, it is easy to identify and model them. However, a close look at the local spectrum showed that peaks may not always be stand-alone but a combination of multiple. Again, automatic deconvolution may help identify all potential peaks but leads to multiple combinations and not always a unique solution.

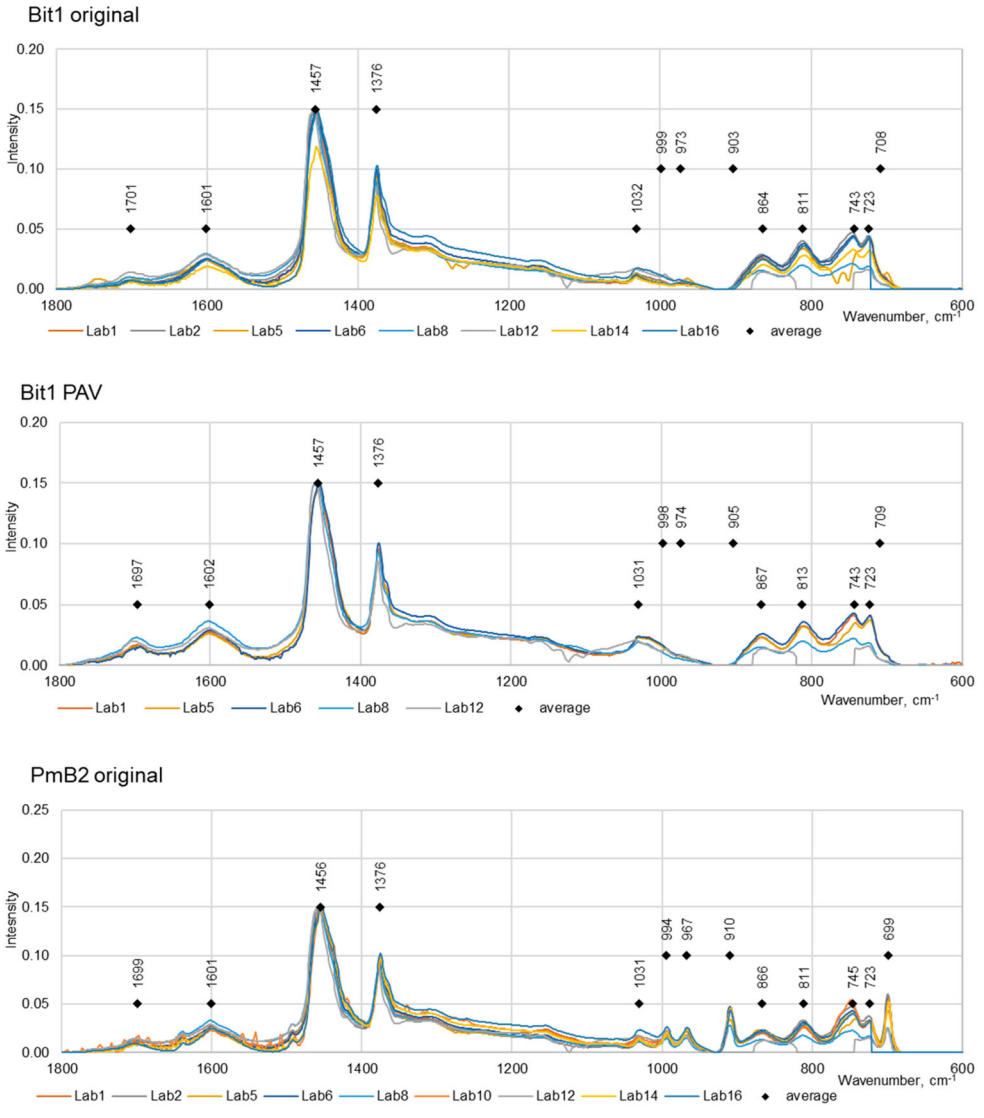

Figure 12. Fitted IR spectra for both binders for all laboratories.

Breakdown of spectrum

A typical IR spectrum usually displays two regions. Between 4000 and 2000 cm^{-1}, the left half has relatively few but high sharp peaks, most likely alkane, C–H stretching, either from saturated or unsaturated groups. The region between 2800 and 1800 cm^{-1} is usually flat with limited absorption peaks. The right half, between 2000 and 600 cm^{-1}, has many different absorption peaks of different intensities. Some of them are isolated and easy to be identified, while others are a combination of multiple peaks. The central part has high sharp peaks, while the others have lower broad peaks.

For further analysis, the whole spectrum was analysed in a close look with five blocks. These blocks were determined to be independent of each other and with characteristic absorption peaks displaying similar amplitude. Figure 13 shows the breakdown of the whole spectrum with,

- Block 1, from 3200 to 2600 cm^{-1}, related to alkyl groups

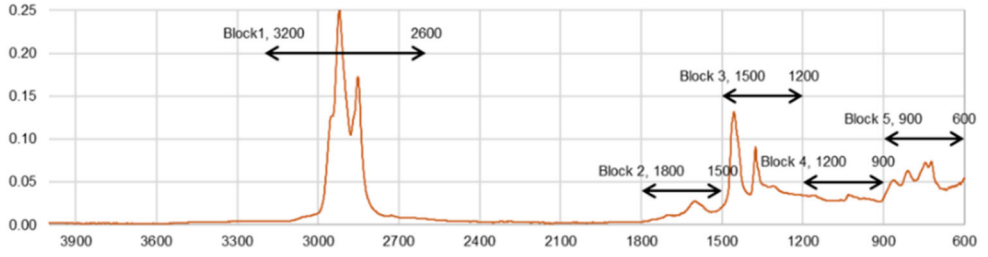

Figure 13. Breakdown of IR spectrum for fingerprint analysis.

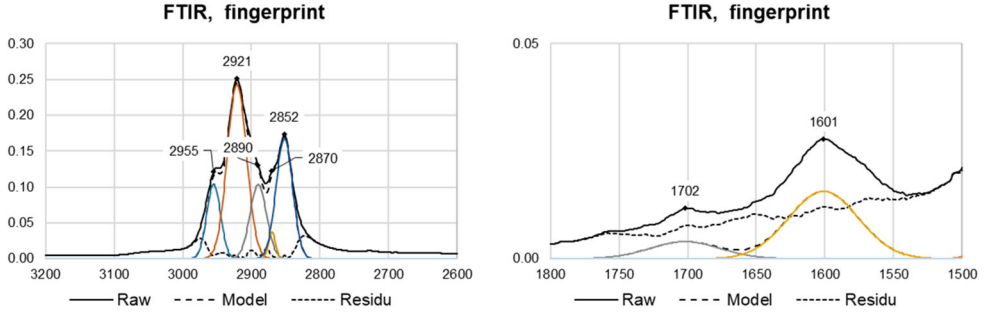

Figure 14. Examples of peak deconvolution.

- Block 2, from 1800 to 1600 cm^{-1}, to locate the carbonyl groups
- Block 3, from 1500 to 1200 cm^{-1}, mostly with aliphatic groups
- Block 4, from 1200 to 900 cm^{-1}, a broad band including sulfoxide and potential groups present in styrene and butadiene
- Block 5, from 900 to 600 cm^{-1}, with multi peaks including aromatic groups

Deconvolution approach

Each main absorption peak was first identified by its wavelength number intensity of the peak. A local baseline, valley-to-valley, was determined and the height of the peak, above this local baseline, was used to determine the theoretical shape factor σ, as per Gaussian curve, at 0.6 of the bell curve, where the curve inflexions are located. In the case of multiple peaks, iteration was made by first identifying the main absorption peak. Then, by subtracting this peak curve from the full measurement, a residual spectrum helped to identify the secondary absorption peaks, often on the shoulder or the main peak. Figure 14 shows examples of this peak identification approach for block 1 with multiple peaks and block 2 with single peaks. The black plain curve is for the raw data, the black dotted line for the modelled spectrum, the black point line for the residue, the difference between the raw and model data points, and the other curves, in colours, for the individual peaks. The computation has been done in a systemic approach to minimise the residue within the baseline. From this interpretation, it is clear that, for a combination of peaks, the maximum peak may hide secondary peaks, which at the end are not negligible. In addition, the residual curve follows closely the baseline used to identify the peaks.

FTIR fingerprint for bituminous binder

The approach was applied for Bit1 on five laboratory raw data sets, where the outlier laboratories were not taken into account. For each laboratory, per block, the fingerprint was determined to minimise as

Table 6. Fingerprint model for Bit1 (average from 5 laboratories).

Functional group	Bond vibration	Location, cm^{-1}	Semi-width	Intensity
Alkyl	C-H asymmetric	2950 ± 1.5	11 ± 0.9	$4.6 \pm 45\%$
	C-H	2920 ± 1.2	14 ± 0.0	$11.6 \pm 28\%$
		2890 ± 2.2	13 ± 1.3	$4.5 \pm 36\%$
		2870 ± 0.4	5 ± 0.0	$0.6 \pm 30\%$
	C-H symmetric	2850 ± 1.3	12 ± 0.0	$6.6 \pm 20\%$
Carbonyl	C = O	1704 ± 1.6	13 ± 7.9	$0.15 \pm 69\%$
Aromatic	C = C	1602 ± 1.3	24 ± 3.1	$1.1 \pm 18\%$
Aliphatic	CH2	1456 ± 1.7	13 ± 1.2	$4.3 \pm 27\%$
		1435 ± 1.8	8 ± 2.6	$0.5 \pm 76\%$
	CH3	1376 ± 0.0	5 ± 0.4	$0.8 \pm 24\%$
		1365 ± 0.4	6 ± 5.3	$0.3 \pm 44\%$
		1158 ± 6.1	14 ± 4.5	$0.13 \pm 48\%$
Sulfoxide	S = O	1030 ± 0.5	6 ± 0.5	$0.09 \pm 37\%$
		1017 ± 4.1	6 ± 2.3	$0.07 \pm 81\%$
		866 ± 1.1	19 ± 0.4	$1.2 \pm 39\%$
Aromatic	C-CH	811 ± 1.4	16 ± 1.2	$1.3 \pm 32\%$
		769 ± 6.1	15 ± 4.5	$0.7 \pm 60\%$
Aromatic	C-CH	744 ± 3.2	10 ± 3.1	$0.9 \pm 77\%$
Long chain		722 ± 0.4	7 ± 1.5	$0.6 \pm 28\%$

much as possible the residue and at the same time to optimise the number of peaks. In total, on Bit1, about 20 peaks were identified, five between 3200 and 2600 cm^{-1}, two between 1800 and 1500 cm^{-1}, four between 1500 and 1200 cm^{-1}, two between 1200 and 900 cm^{-1} although the sulfoxide can be added as well, and five between 900 and 600 cm^{-1}. For each absorption peak, the wavelength number, the semi-width as per Gaussian bell-curve shape parameter, σ, and the total area were determined. Table 6 displays these parameters for each absorption peak, with an average value and standard deviation, or relative variation for the intensity.

Most often, the locations of the absorption peaks were of good prediction within $\pm 2\ cm^{-1}$. The semi-width was in reasonable reproducibility within $\pm 2\ cm^{-1}$ variation. When it was higher, it was linked with a small absorption peak intensity. For example, the carbonyl peak around 1700 cm^{-1} had an average half-width or 13 cm^{-1} $\pm 8\ cm^{-1}$ for an intensity of 0.15. However, for the original bitumen, the carbonyl peak as seen on spectra was almost null.

Finally, the absorption intensity displayed the greatest variation in a range of 20%–80%. This is not surprising as the considered raw data from different laboratories had different intensities that can be observed between the spectra.

The analysis was made on raw data in order to identify any relevant variability between laboratories. Overall, from these five spectra on one binder, a specific fingerprint can be defined using wavelength number and absorption peak width. The intensity is more laboratory-dependent. Figure 15 shows the typical theoretical modelled fingerprint for Bit1. From the 20 absorption peaks initially modelled, the fingerprint may be further simplified by removing or combining small secondary peaks. This simplified fingerprint can be based on 15–16 absorption peaks. Knowing absorption peak wavelength number and width, the intensities for each peak can be determined using solver tools to best fit the raw spectrum.

The overall analysis was extended to the seven binders from one laboratory. It provided a similar typical fingerprint for bitumen. The same source of bitumen was used and helped identify additional most common absorption peaks from modifiers, with ester group around 1740 cm^{-1}, functional groups from butadiene or styrene around 990, 965, 910 and 700 cm^{-1}. This fingerprint approach can be further used as a platform when analysing FTIR data set for various bituminous binders or between different laboratory results. It may be useful to extend the analysis to neat binders from different sources or processes to assess the robustness of the model, especially with regards to the semi-width parameter.

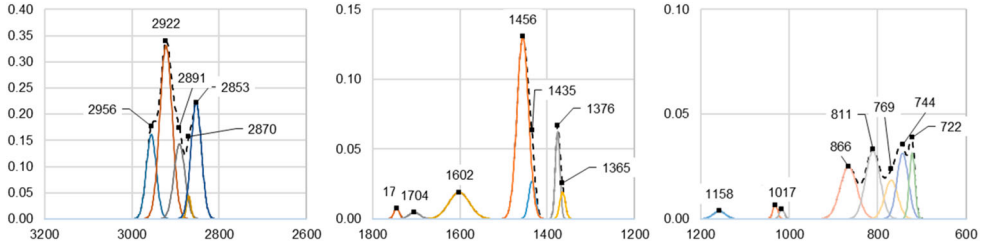

Figure 15. Typical fingerprint for neat bitumen.

Conclusion

Fourier Transform Infrared, FTIR, spectroscopy is a well-established and used analytical tool to characterise bituminous binder. It is a simple and fast measurement technique. However, the reproducibility between different laboratories often leads to variability of the spectrum. FTIR analysis may benefit from having further treatment of the raw data for a standardised interpretation.

Within the inter-laboratory experimental programme from the RILEM TC 272 PIM TG1, eleven laboratories generated FTIR data on seven different bituminous binders at three different ageing conditioning. The direct comparison of all spectra did show variability in results. However, a first analysis using Gaussian normal distribution and, more specifically, the use of the 1st derivative highlighted good consistency of measurement between laboratories. The absorption peaks may be located at the same wavelength number consistently with a variation of less than 2 cm^{-1}. Similarly, at the limits for specific peaks, a close look up showed good reproducibility between laboratories with a variation of less than 10% for the peaks span.

In order to visually compare spectra of different laboratories, a specific fitting model was developed. First, a baseline adjustment is applied using eight points at 4000, 3600, 3100, 2400, 1800, 930, 680 and 600 cm^{-1}. This enables offsetting any potential noise generation from laboratory to laboratory. The second proposed step is normalising the spectrum from the maximum peak between 1800 and 600 cm^{-1} over 0.15 intensity. This normalisation provided the best fitting between laboratories for characteristic bands used for analysis. This fitting model enables to have a qualitative analysis of spectra when comparing different laboratory results.

Finally, a simplified, but controlled, deconvolution model was developed based on Gaussian normal distribution. The analysis was made per block to best identify single peaks or a combination of multiple peaks. Depending on the degree of granularity for the analysis, between 20 and 15 peaks have been identified for the fingerprint of neat bitumen. With a more complex bituminous binder, additional absorption peaks will be easier to identify and qualify. The fingerprint is based on the wavelength number and width of each absorption peak, which are foreseen as intrinsic peak parameters regardless of the laboratory measurements. Further, using solver tools, the intensity of each peak can be easily determined to best fit the raw spectra. This typical fingerprint has been established on one binder between five laboratories and confirmed on the seven binders from one laboratory. It would be necessary to extend the proposed methodology to various neat bitumen from different sources or processes to address the robustness of the model.

This fundamental approach can serve as a platform for further analysis and interpretation of FTIR spectra of bituminous binders. The next step will be applying peak intensity to quickly determine various indexes either from oxidation or from the presence of modifiers in the binders.

Acknowledgement

This work has been conducted under the framework of the RILEM Technical Committee TC 272-PIM on 'Phase and Interphase behaviour of innovative bituminous Materials' with the great contribution of Kraton (NL), Western Research Institute (US), University of New Hampshire (US), Université Gustave Eiffel (FR), TU Delft (NL), Institute of Transportation

TU Wien (AU), FHWA (US), Cerema Méditerranée (FR), Colas CST (FR), Strukton (NL), Politecnico di Torino (IT), Belgian Road Research Centre (BE), Swedish National Road and Transport Research Institute (SW), Nynas and University of Antwerp (BE), Nebraska DoT (US), Aalto University (FI), Institut für Straßenwesen, Technische Universität Braunschweig (DE).

Disclosure statement

No potential conflict of interest was reported by the author(s).

ORCID

Laurent Porot http://orcid.org/0000-0002-7173-9035
Panos Apostolidis http://orcid.org/0000-0001-5635-4391

References

Abramowitz, S., & Bauman, R. (1963). Measurement of infrared band contours in solution. *The Journal of Chemical Physics*, *39*(10), 2757–2767. https://doi.org/10.1063/1.1734094

Adams, J., Elwardany, M., Planche, J., Boysen, R., & Rovani, J. (2019). Diagnostic techniques for various asphalt refining and modification methods. *Energy & Fuels*, *33*(4), 2680–2698. https://doi.org/10.1021/acs.energyfuels.8b03738

Apostolidis, P., Elwardany, M., Porot, L., Vansteenkiste, S., & Chailleux, E. (2021). Glass transitions in bituminous binders. *Materials and Structures*, *54*(132). https://doi.org/10.1617/s11527-021-01726-6

ASTM. (2016). *ASTM e168 – Standard practices for general techniques of infrared quantitative analysis*. ASTM International.

Cannone Falchetto, A., Porot, L., Riccardi, C., Hugener, M., Tebaldi, G., & Dave, E. (2019). Effects of rejuvenator on reclaimed asphalt binder: An exploratory study of the RILEM TC 264-RAP task group 3. In *RILEM 252-CMB symposium* (pp. 295–200). Braunschweig. https://doi.org/10.1007/978-3-030-004767-7_31

Dony, A., Ziyani, L., Drouadaine, I., Pouget, S., Faucon-Dumont, S., Simard, D., Mouillet, V., Poirier, J. E., Gabet, T., Boulangé, L., Nicolaï, A., & Guiet, C. (2016). MURE national project: FTIR spectroscopy study to assess ageing of asphalt. In *5th e&E congress* (p. 154). https://doi.org/10.14311/EE.2016.154

Dorrence, S., Barbour, F., & Petersen, J. (1974). Direct evidence of ketones in oxidised asphalts. *Analytical Chemistry*, *46*(14), 2242–2244. https://doi.org/10.1021/ac60350a003

Geng, W., Nakajima, T., Takanashi, H., & Ohki, A. (2009, January). Analysis of carboxyl group in coal and coal aromaticity by Fourier transform infrared (FT-IR) spectrometry. *Fuel*, *88*(1), 139–144. https://doi.org/10.1016/j.fuel.2008.07.027

Glaser, R., Turner, T., Loveridge, J., Salmans, S., & Planche, J.-P. (2015). *Fundamental properties of asphalts and modified asphalts III product: FP10 and 11*. Western Research Institute.

Hofko, B., Alavi, M., Grothe, H., Jones, D., & Harvey, J. (2017). Repeatability and sensitivity of FTIR ATR spectral analysis methods for bituminous binders. *Materials and Structures*, *50*(3), 187. https://doi.org/10.1617/s11527-017-1059-x

Hofko, B., Porot, L., Falchetto Cannone, A., Poulikakos, L., Huber, L., Lu, X., Mollenhauer, K., & Grothe, H. (2014). FTIR spectral analysis of bituminous binders: Reproducibility and impact of ageing temperature. *Materials and Structures*, *51*(8), 1273–1286. https://doi.org/10.1617/s11527-018-1170-7

Jemison, H., Burr, B., Davison, R., Bullin, J., & Glover, C. (1992). Application and use of the ATR, FT-IR method to asphalt aging studies. *Fuel Science and Technology International*, *10*(4-6), 795–808. https://doi.org/10.1080/08843759208916021

Lamontagne, J., Dumas, P., Mouillet, V., & Kister, J. (2001). Comparison by Fourier transform infrared (FTIR) spectroscopy of different ageing techniques: Application to road bitumens. *Fuel*, *80*(4), 483–488. https://doi.org/10.1016/S0016-2361(00)00121-6

Lopes, M., Mouillet, V., Bernucci, L., & Gabet, T. (2016). The potential of attenuated total refection imaging in the mid infrared to study recycled asphalt mixtures. *Construction and Building Materials*, *124*, 1120–1131. https://doi.org/10.1016/j.conbuildmat.2016.08.108

Maddams, W. (1980). The scope and limitations of curve fitting. *Applied Spectroscopy*, *34*(3), 245–267. https://doi.org/10.1366/0003702804730312

Margaritis, A., Soenen, H., Fransen, E., Pipintakos, G., Jacobs, G., Blom, J., & Van den bergh, W. (2020). Identification of ageing state clusters of reclaimed asphalt binders using principal component analysis (PCA) and hierarchical cluster analysis (HCA) based on chemo-rheological parameters. *Construction and Building Materials*, *244*, 118276. https://doi.org/10.1016/j.conbuildmat.2020.118276

Marsac, P., Pierard, N., Porot, L., Van der Bergh, W., Grenfell, J., Mouillet, V., Pouget, S., Besamusca, J., Farcas, F., Gabet, T., & Hugener, M. (2014, August). Potential and limits of FTIR methods for reclaimed asphalt characterisation. *Materials & Structures*, *47*(8), 1273–1286. https://doi.org/10.1617/s11527-014-0248-0

Masson, J., Pelletier, L., & Collins, P. (2001). Rapid FTIR method for quantification of styrene-butadiene type copolymers in bitumen. *Journal of Applied Polymer Science*, *79*(6), 1034–1041. https://doi.org/10.1002/1097-4628(20010207)79:6 < 1034::AID-APP60 > 3.0.CO

Mouillet, V., Farcas, F., Battaglia, V., Besson, S., Petiteau, C., & Lecunff, F. (2010). Identification and quantification of bituminous binder's oxygenated species, Analysis by Fourier Transfrom Infrared Spectroscopy. In *LCPC testing method 69 Technical report ME69* (Ed.). LCPC.

Mouillet, V., Lamontagne, J., Durrieu, F., Planche, J., & Lapalu, L. (2008). Infrared microscopy investigation of oxidation and phase evolution in bitumen modified with polymers. *Fuel*, *87*(7), 1270–1280. https://doi.org/10.1016/j.fuel.2007.06.029

Oreskovic, M., Porot, L., Trifunovic, S., & Mladenovic, G. (2020). Empirical, rheological and chemical properties of aged binder with rejuvenators at different ageing levels. In In *RILEM Bookseries ISBM – Rilem symposium* (Vol. 27, pp. 21–27). Spinger: Lyon.

Partl, M., Bahia, H., Canestrati, F., de la Roche, C., Di Benedetto, H., Piber, H., & Sybilski, D. (2013). *Advances in interlaboratory testing and evaluation of bituminous materials* (Vols. State of the Art report of the RILEM Technical Committee 206-ATB). Springer.

Partl, M., Porot, L., Di Benedetto, H., Canestrari, F., Marsac, P., & Tebaldi, G. (2018). *Testing and characterization of sustainable innovative bituminous materials and systems – State-of-the-art report of the RILEM 237-SIB (Vol. 24)* (RILEM, ed.). Spinger. https://doi.org/10.1007/978-3-319-71023-5

Petersen, J. C. (1975). Quantitative method using differential infrared spectrometry for the determination of compound types absorbing in the carbonyl region in asphalts. *Analytical Chemistry*, *47*(1), 112–117. https://doi.org/10.1021/ac60351a037

Petersen, J. C. (1986). Quantitative functional group analysis of asphalts using differential infrared spectrometry and selective chemical reactions – Theory and application. *Transportation Research Record*(1096), 1–11.

Pierard, N. (2013). *Bitumen analysis with FTIR spectrometry: Processing of FTIR spectra*. BRRC.

Pipintakos, G., Ching, V., Soenen, H., Sjovall, P., Muhlich, U., Van Doorslaer, S., Varveri, A., Van den bergh, W., & Lu, X. (2020, November). Experimental investigation of the oxidative ageing mechanisms in bitumen. *Construction and Building Materials*, *260*, 119702. https://doi.org/10.1016/j.conbuildmat.2020.119702

Porot, L., Chailleux, E., Apostolidis, P., Zhu, J., Margaritis, A., & Tsantilis, L. (2020). *Complex bituminous binders, are current test methods suitable for?* ISBM.

Porot, L., Huguener, M., & Cannone Falchetto, A. (2020). Aging of rejuvenated RAP binder – A RILEM inter-laboratory study. In *7th eurobitume & Eurasphalt* (p. 163).

Porot, L., Vansteenkiste, S., Makowska, M., Carbonneau, X., Zhu, J., Damen, S., & Plug, K. (2021). Characterisation of complex polymer modified bitumen with rheological parameters. *Road Materials and Pavement Design*, *22*, S297–S309. https://doi.org/10.1080/14680629.2021.1910070

Roads & Maritime Services. (2012). *Quantifying of polymer modified binders using infrared spectrum.* https://www.rms.nsw.gov.au/business-industry/partners-suppliers/documents/test-methods/t521.pdf

Seshadri, K., & Norman, R. (1963). The shapes and intensities of infrared absorption bands—A review. *Spectrochimica Acta*, *19*(6), 1013–1085. https://doi.org/10.1016/0371-1951(63)80187-3

Weigl, S., Gehrke, M., Recknagel, C., & Stephan, D. (2021, May). Identification and quantification of additives in bituminous binders based o FTIR spectroscopy and multivariate analysis methods. *Materials and Structures*, *57*(171). https://doi.org/10.1617/s11527-021-01763-1